Published in final edited form as:
Sci Signal. ; 13(656): . doi:10.1126/scisignal.aaz4003.

Gβγ is a direct regulator of endogenous p101/p110γ and p84/p110γ PI3Kγ complexes in mouse neutrophils#

Natalie K. Rynkiewicz[1,†], **Karen E. Anderson**[1,†], **Sabine Suire**[1], **Daniel M. Collins**[1], **Eleftherios Karanasios**[1], **Oscar Vadas**[2,‡], **Roger Williams**[2], **David Oxley**[1], **Jonathan Clark**[1], **Len R. Stephens**[1,*], **Phillip T. Hawkins**[1,*]

[1]Signalling Programme, Babraham Institute, Babraham Research Campus, Cambridge CB22 3AT, UK

[2]MRC Laboratory of Molecular Biology, Francis Crick Avenue, Cambridge Biomedical Campus, Cambridge CB2 0QH, UK

Abstract

The PI3Kγ isoform is activated by Gi-coupled GPCRs in myeloid cells, but the extent to which the two endogenous complexes of PI3Kγ, p101/p110γ and p84/p110γ, receive direct regulation through Gβγ or indirect regulation through RAS and the sufficiency of those inputs is controversial or unclear. We generated mice with point mutations that prevent Gβγ binding to p110γ (RK552DD) or to p101 (VVKR777AAAA) and investigated the effects of these mutations in primary neutrophils and in mouse models of neutrophilic inflammation. Loss of Gβγ binding to p110γ substantially reduced the activation of both p101/p110γ and p84/p110γ in neutrophils by various GPCR agonists. Loss of Gβγ binding to p101 caused more variable effects, depending on both the agonist and cellular response, with the biggest reductions seen in PIP3 production by primary neutrophils in response to LTB4 and MIP-2 and in the migration of neutrophils during thioglycolate-induced peritonitis or MIP2-induced ear pouch inflammation. We also observed that $p101^{VVKR777AAAA}$ neutrophils showed enhanced p84-dependent ROS responses to fMLP and C5a, suggesting that competition may exist between p101/p110γ and p84/p110γ for Gβγ subunits downstream of GPCR activation. GPCRs did not activate p110γ in neutrophils from mice lacking both the p101 and p84 regulatory subunits, indicating that RAS binding to p110γ is insufficient to support GPCR activation in this cell type. These findings define a direct role for Gβγ subunits in

*Equal senior authors and to whom correspondence should be addressed: len.stephens@babraham.ac.uk; phillip.hawkins@babraham.ac.uk.
†These authors contributed equally
‡Current address: Faculty of Medicine, Department of Microbiology and Molecular Medicine CMU, 1 rue Michel-Servet CH-1211 Genève 4, Switzerland.

Author contributions
N.K.R., K.E.A., S.S., D.M.C., and E.K. performed experiments; J.C. and D.O. analyzed lipidomic and proteomic samples respectively. N.K.R., K.E.A., E.K., S.S., P.T.H., and L.R.S. analyzed data; O.V. and R.W. supplied important resources and information; P.T.H., N.K.R., K.E.A., S.S., L.K., and L.R.S. designed research; and P.T.H., K.E.A., N.K.R., S.S. and L.R.S. wrote the article.

Competing interests
The authors declare that they have no competing interests.

Europe PMC Funders Author Manuscripts

activating both of the endogenous PI3Kγ complexes and indicate that the regulatory PI3Kγ subunit biases activation towards different GPCRs.

Introduction

The class I phosphoinositide 3-kinase (PI3K) signaling pathway is an important component of the regulatory network that allows activated cell surface receptors to control several essential aspects of cell function, such as growth, movement and survival (1). PI3Kγ is a class I PI3K isoform with a restricted tissue expression in vertebrates. PI3Kγ is highly expressed in cells of haematopoetic origin, with a well-established role in myeloid cells, although it also has a role in other cell types, such as myocytes, endothelial cells and neurons (2). PI3Kγ is a heterodimer composed of a common p110γ catalytic subunit and one of two potential regulatory subunits, p84 (also known as p87) or p101, resulting in two endogenous complexes, p101/p110γ or p84/p110γ (2). The p110γ subunit catalyzes the phosphorylation of the inositol phospholipid phosphatidylinositol 4,5-bisphosphate [$PI(4,5)P_2$] in the plasma membrane to form phosphatidylinositol 3,4,5-trisphosphate [$PI(3,4,5)P_3$] (PIP_3) (3). PIP_3 regulates the location and function of a complex network of effector proteins, such as AKT/protein kinase B (PKB), Bruton's tyrosine kinase (BTK), and PIP_3-dependent RAC exchanger 1/2 (PREX1/2), which transduce the signal from the activated receptor to intracellular locations (1).

PI3Kγ was initially characterized as a p101/p110γ heterodimer that was potently activated by Gβγ subunits (4), and thus was potentially the PI3K isoform that coupled heterotrimeric G protein -coupled receptors (GPCRs) to the formation of PIP_3. This notion was subsequently confirmed by studies with *p110γ*-knockout (*p110γ*-KO) mice, which demonstrated that p110γ is required for Gi-linked GPCRs to stimulate PIP_3-dependent signaling in myeloid cells, such as neutrophils (5) (6) (7). p84 was later discovered by homology cloning and forms an alternative p84/p110γ heterodimer (8) (9) with an overlapping but distinct tissue distribution and function in specific cell types, such as mast cells and cardiomyocytes (2) (10). Studies using catalytic-site inhibitors of p110γ or *p110γ*-KO and *p110γ* kinase-dead knock-in mice have defined important roles for PI3Kγ catalytic activity in the normal inflammatory response to injury and infection and in pathophysiological responses to inflammatory disease (11) (12) (13). PI3Kγ also plays important roles in creating a permissive tumor microenvironment and in supporting tumor metastasis, a finding that has reinvigorated efforts to target this enzyme therapeutically (14) (15, 16).

Biochemical assays using recombinant proteins, supported by heterologous expression in model cell systems, have described two direct activators of PI3Kγ complexes, Gβγ and guanosine 5'-triphosphate (GTP)-loaded RAS (GTP-RAS), although other direct regulators may also exist, such as RAB8a (2) (17). There appears to be general agreement that p101/p110γ is more sensitive to activation by Gβγ than p84/p110γ, but the extent to which p84/p110γ is more sensitive than p110γ alone is unclear (2) (8). There is also general agreement that GTP-RAS binds directly to the RAS-binding domain (RBD) of p110γ and can elicit modest activation of p110γ alone, but can also act in synergy with Gβγ to promote more

Europe PMC Funders Author Manuscripts

effective activation of p101/p110γ and p84/p110γ complexes (18–20). Some of these studies have been interpreted to suggest GTP-RAS is an indispensable regulator of p84/p110γ, but Gβγ is a more important regulator of p101/p110γ(21), though evidence for a qualitative distinction in vivo is lacking.

p84 and p101 also direct signaling downstream of p110γ. Thus, neutrophils lacking p84 have selective defects in p110γ-dependent oxidase activation but neutrophils lacking p101 show selective defects in p110γ-dependent motility, despite both subunits supporting similar levels of GPCR-stimulated PIP_3-formation and phosphorylation of PKB(22). In analogous studies, p84 and p101 have differential effects on mast cell secretion and migration(23), and p84/p110γ and p101/p110γ complexes appear to have differential roles downstream of Toll-like receptors and receptor tyrosine kinases(17, 24, 25). The molecular basis for these selective roles is unknown, as is their relationship to potential differences in upstream regulation. p101/p110γ and p84/p110γ complexes have been suggested to exist in distinct ‘nanodomains’ and/or act as scaffolds for effectors, a concept supported by the discovery of noncatalytic roles for p84/p110γ, such as acting as a scaffold for phosphodiesterase 3 (PDE3) and PKA in cardiomyocytes(26).

A major problem in relating biochemical and model cell studies to the properties of p101/p110γ and p84/p110γ in vivo is the difficulty in recreating the endogenous environment, including the relative abundance of all relevant molecules (for instance, PI3Kγ subunits and their immediate regulators) and a native plasma membrane (the biophysical properties of the lipid environment are critical for determining access to substrate and enzyme conformation) (2, 18, 20). Thus, for many of the observed in vitro properties, they suggest what may happen, not what does happen in a given physiological context. The most direct way of interrogating the relative roles of specific regulatory inputs in vivo is to define knock-in mutations that selectively interfere with these regulatory inputs, which usually requires a combination of structural and biochemical information.

A crystal structure is available for GTP-RAS bound to the RBD of p110γ, which has allowed the definition of mutations that selectively block activation of p110γ by GTP-RAS, but which do not affect Gβγ-activation of p110γ alone or in complex with a regulatory subunit(19). Data obtained with mice bearing these knock-in mutations (*p110γ*-RBD) has shown an unexpectedly important role for GTP-RAS in regulating both p84/p110γ- and p101/p110γ-dependent signaling downstream of GPCRs in primary neutrophils (22, 27), in apparent contradiction with data obtained from some in vitro assays (2).

No crystal structures are available for the p84 or p101 regulatory subunits, either alone or in complex with p110γ or Gβγ, which has severely hampered attempts to understand the role of Gβγ in activating these complexes. However, a study combining hydrogen-deuterium exchange mass spectroscopy (HDX-MS), mutagenesis, biochemical assays and heterologous expression in model cells has provided information on the surfaces through which these proteins interact, both with each other and with a model membrane(20). This work shows that Gβγ binds to a site in p110γ in the p84/p110γ complex but describes additional interactions between Gβγ and p101 in the p101/p110γ complex, potentially explaining the latter’s greater sensitivity to Gβγ. This study has also defined mutations which selectively

interfere with Gβγ binding to p110γ (RK552DD) and p101(VVKR777AAAA), which, alone and in combination, block Gβγ-activation of p84/p110γ and p101/p110γ, respectively(20).

We generated mice which carried the p110γ^{RK552DD} and p101^{VVKR777AAAA} mutations, to assess the role of Gβγ in activating endogenous complexes of PI3Kγ. We also generated mice lacking both p84 and p101 regulatory subunits to assess a potential role for GTP-RAS in activating monomeric p110γ. We focused on characterizing the effects of these genetic manipulations on Gi-coupled GPCR signaling in primary neutrophils, because this is the cell type in which the largest body of relevant information currently exists to aid interpretation of our results.

Results

Genetically engineered mice

Mice lacking both regulatory subunits of PI3Kγ *(p101/p84*-dKO (double knockout)); knock-in mutations in both alleles of p110γ (RK552DD; *p110γ*-Gβγ); knock-in mutations in both alleles of p101 (VVKR777AAAA; *p101*-Gβγ) or, both alleles of both genes (*p110γ/p101*-dGβγ), were generated (figs. S1, A to D, S2, A to D, and S3, A to D). The p110γ-Gβγ mutation ablates activation of p110γ or p84/p110γ by Gβγ in vitro, but has only a partial effect on Gβγ activation of p101/p110γ(20). The p101-Gβγ mutation has a strong but incomplete effect on activation of p101/p110γ by Gβγ in vitro, but dual p101-Gβγ and p110γ-Gβγ mutation effectively blocks activation of this complex by Gβγ(20). These knock-in mutations selectively interfere with Gβγ activation but do not affect basal activity or activation by GTP-RAS(20). These findings are summarized in Fig.1A.

These genetically engineered mice appeared normal and offspring were generated from hybrid crosses at the expected Mendelian ratios. Blood counts were also within normal ranges (table S1). Neutrophils were isolated from the bone marrow of adult mice (8 to 12 weeks) and expression levels of the various PI3Kγ subunits were assessed by Western Blotting (Fig. 1, B to E). Comparisons were also made with neutrophils isolated from previously established mice: *p110γ*-KO, *p101*-KO, *p84*-KO and *p110γ*-RBD (in which the binding site for GTP-RAS is mutated). Loss of both p84 and p101 regulatory subunits had only a small effect on expression of p110γ (< 20%). Loss of p110γ, however, reduced expression of both p84 and p101. These results agree with previous data indicating that the catalytic subunit is relatively stable in the absence of the regulatory subunits, but the converse is not true(2). The p110γ-Gβγ mutation did not significantly affect expression of p110γ or either regulatory subunit. The p101-Gβγ mutation did not significantly affect expression of p101, p110γ or p84. Further, the p110γ/p101-dGβγ double mutation behaved similarly with respect to subunit expression levels compared to the single mutations.

PIP_3 responses in isolated neutrophils

We measured PIP_3 formation in response to several GPCR agonists in bone marrow-derived neutrophils isolated from the mouse genotypes created in this study. In response to 10μM Nformyl-Met-Leu-Phe (*f*MLP), PIP_3 showed a characteristic biphasic accumulation,

peaking at about 10 s (Fig. 2A). PIP_3 accumulation was reduced in *p101/p84*-dKO neutrophils to the level seen in *p110γ*-KO neutrophils (Fig. 2, A and B, and fig. S4, A and B). Thus, in the absence of a regulatory subunit, p110γ is insufficient to support activation by *f*MLP in this assay. PIP_3 accumulation in *p110γ*-Gβγ neutrophils was about 45% of the wild type (WT), with similar kinetics (Fig. 2, A and B, and fig. S4D), defining a substantial, nonredundant role for Gβγ binding to p110γ in the activation of endogenous PI3Kγ complexes. The PIP_3 response of *p101*-Gβγ neutrophils was similar to that of WT neutrophils (Fig. 2, A and B, and fig. S4C) but significantly less in *p110γ/p101*-dGβγ neutrophils compared to *p110γ*-Gβγ neutrophils (Fig. 2, A and B, and fig. S4, D and E), suggesting that direct binding of Gβγ to p101 can play a role in p110γ-activation by *f*MLP, but that this role is not essential in the presence of Gβγ binding to p110γ.

The apparent lack of effect of the p101-Gβγ mutation alone was unexpected, given the substantial effect this mutation has in in vitro assays(20). We therefore measured PIP_3 responses to submaximal and near maximal (about 80%) doses of *f*MLP and macrophage inflammatory protein-2 (MIP-2), a near maximal dose of LTB4 and C5a, and a maximal dose of surfen [also known as 12155; a small molecule that displaces Gβγ from Gi without promoting guanine nucleotide exchange on the αi subunit (28)] (Fig. 2, C and D). The p101-Gβγ mutation significantly reduced PIP_3 accummulation by about 20-25% in response to MIP-2 (at either dose) or LTB4 but had no significant effect on responses to *f*MLP or C5a (Fig. 2C). Moreover, this reduction in the MIP-2 response was similar at each of the different times analyzed (Fig. 2E). The p101-Gβγ mutation also reduced the PIP_3 response to surfen by about 25% (Fig. 2D). These results suggest the Gβγ-p101 interaction plays a more important role in the activation of endogenous PI3Kγ by some receptors compared to others.

PKB, PLC and ERK responses in isolated neutrophils

We also measured the effect of the Gβγ-binding mutations on other responses to *f*MLP in isolated neutrophils. The phosphorylation of Ser^{473} in PKB followed a similar pattern to that seen with the PIP_3 measurements, with significant reductions seen in the *p110γ*-Gβγ and *p110γ/p101*-dGβγ mutants (Fig. 2F). These findings are consistent with previous work indicating phosphorylation of this site follows PIP_3-formation by both p84/p110γ and p101/p110γ complexes in *f*MLP-stimulated neutrophils (22).

*f*MLP-stimulated formation of diacylglycerol (DAG) (a relatively direct measure of PLCβ2/3 activity) and phosphorylation of extra-cellular signal-regulated kinase (ERK)1/2 (an indirect measure of RAS activity downstream of PLCβ2/3) (29) were not significantly affected by the Gβγ-binding mutants (Fig. 2, G and H). Although the variance in some of this data does not exclude minor effects, these results suggest the Gβγ-binding mutations do not have a large, confounding effect on the activation of PI3Kγ through an indirect effect on RAS.

Reactive oxygen species responses in isolated neutrophils

The activation of the neutrophil oxidase by Gi-coupled receptors is coordinated by several interconnected signal transduction pathways, including PI3K, PLC, RAC and ERK. This

signaling network is incompletely understood and the relative magnitude of responses depends heavily on the nature of the neutrophil isolation protocol and prior exposure to 'priming' factors (such as lipopolysccharide). Under our conditions, reactive oxygen species (ROS) responses to *f*MLP, C5a, LTB4 and MIP-2 exhibited a wide range of magnitudes and kinetics (Fig. 3A).

The mutations created in this study did not significantly impact the activation of the oxidase by phorbol 12-myristate 13-acetate (PMA) (Fig. 3B), a treatment considered to bypass upstream regulatory pathways by directly driving PKC-mediated assembly of an active neutrophil complex. Consistent with this finding, we observed no differences in the expression of the soluble oxidase subunits $p67^{phox}$ and $p47^{phox}$ between our mutants (Fig. 1B and fig. S5).

The ROS response to *f*MLP is regulated by p84/p110γ-dependent PIP_3 formation, with minimal dependence of parallel activation of p101/p110γ (22). ROS formation in response to *f*MLP was ablated in *p101/p84*-dKO neutrophils (Fig. 3C, and fig. S6D, in line with the PIP_3 measurements described above and previous studies with *p110γ*-KO neutrophils. ROS formation was also substantially reduced (~50%) in *p110γ*-Gβγ neutrophils and to a similar extent in *p110γ/p101*-dGβγ neutrophils (Fig. 3C, and fig. S6, B and C). This finding is in contrast with the PIP_3 data, in which the double knock-in exhibited a larger defect, but is consistent with the lack of involvement of the p101/p110γ complex in oxidase activation. We also observed a variable but large increase in ROS formation in *p101*-Gβγ neutrophils (~250% increase, with similar kinetics; Fig 3C, and fig S6A).

We also investigated the effects of the Gβγ-binding mutations on the ROS responses to C5a (Fig. 3D), LTB4 (Fig. 3E) and MIP-2 (Fig. 3F). Despite the wide differences in size and speed of the individual ROS responses, the p110γ-Gβγ mutation, either alone or in combination with the p101-Gβγ mutation, caused similar reductions (~50%) compared to WT. However, the effect of the p101-Gβγ mutation alone was different depending on the agonist, causing an increased response with C5a, no effect with LTB4 and a decrease with MIP-2. Thus, it would seem that the p101-Gβγ mutation has a differential and probably indirect effect on the signaling network depending on the nature of the activating GPCR.

Neutrophil migration in vitro

PI3Kγ supports GPCR-stimulated neutrophil chemotaxis, a role that is most clearly demonstrated by the proportion of motile cells on a fibrinogen surface and has been attributed to p101/p110γ, with little involvement of p84/p110γ (22) (30). In agreement with these studies, we found no significant effect of any of the genotypes on migratory index in response to *f*MLP and only a small reduction in speed for *p101/p84*-dKO and *p110γ*-KO neutrophils (Fig. 4, A and B). However, the proportion of motile cells for both the *p110γ*-Gβγ and *p110γ/p101*-dGβγ neutrophils was reduced by ~50%, similar to that seen for *p110γ*-KO and *p101/p84*-dKO neutrophils (Fig. 4B). No significant effect of the p101-Gβγ mutation was observed in these experiments (Fig.4B).

Neutrophil migration in vivo

We investigated the effects of Gβγ-interaction mutations in p110γ and p101 on neutrophil recruitment in vivo. In both thioglycolate-induced peritonitis and MIP-2-induced ear pouch inflammation, the p110γ-Gβγ, p101-Gβγ and p110γ/p101-dGβγ mutations resulted in an about 50% reduction in neutrophils arriving at sites of inflammation at the times analyzed (Fig. 4, C and D; the effects of these mutations on other immune cell sub-types in induced peritonitis are shown in fig. S7, A and B). These models involve multiple cell types and mediators but indicate a substantial, non-redundant role for Gβγ binding to both p110γ and p101 at some point in the inflammatory cascade in vivo. On the basis of previous studies and the other results presented here, it seems likely a major point of action is GPCR-stimulation of neutrophil extravasation and migration.

p84 and p101 interacting proteins

We attempted to search for endogenous p84- and p101-interacting proteins in mouse neutrophils by expressing HaloTag and green fluorescent protein (GFP)-tagged versions of these subunits in their respective KO backgrounds (fig. S8A). HaloTag-p84 restored ROS formation in response to *f*MLP, indicating it was functionally active (fig. S8B) and both tagged versions were effectively purified on the relevant matrices (fig. S9, A to D). The lists of proteins that were significantly enriched in the target-directed pull-downs compared to WT controls, in the presence or absence of prior stimulation with *f*MLP, and in the presence or absence of paraformaldehyde crosslinking, are shown in tables S2 and S3 (and a selection graphed in fig. S10, A and B). As expected, the p110γ subunit was highly enriched in p84- and p101-directed pull-downs. A higher proportion of p110γ was recovered with HaloTag-p84 when the samples were cross-linked (fig. S10B), suggesting either an effect of the HaloTag or that the p84-p110γ complex is more labile than the p101-p110γ complex, as suggested in some previous studies (31). Several of the isolated proteins are known chaperones or commonly occur in analogous pull-downs with other baits, but we note that several 14-3-3 proteins reproducibly copurified with either p84 or p101 in these experiments. *f*MLP appeared to increase the recovery of some species of 14-3-3 proteins. 14-3-3-proteins are phosphorylation-dependent scaffolds that organize signaling complexes (32). It is thus plausible that they are involved in organizing signaling upstream and/or downstream of PI3Kγ complexes, but confirmation of a role will require substantial further work. We also note the presence of the $p47^{phox}$ (Ncf1) subunit of the neutrophil oxidase in p84-directed pull-downs and of cytoskeletal scaffolds and regulators (such as ankyrin-1 and profilin-1) with p101, which given the role of p84/p110γ in the regulation of the oxidase and of p101/p110γ in the regulation of neutrophil migration, suggests there may be scaffolding of selected effectors downstream of the individual PI3Kγ complexes in neutrophils.

Discussion

We created mice with a dKO of p84 and p101 regulatory subunits through successive rounds of targeting (PIK3R6 and PIK3R5 are neighboring genes on chromosome 17). The expression of p110γ was only minimally affected in neutrophils derived from these mice, but GPCR-stimulated PIP_3 formation, ROS production and motility in *p84/p101*-dKO neutrophils were reduced to the same level as in *p110γ*-KO neutrophils. This finding

suggests that p110γ, in the absence of a regulatory subunit, is insufficient to support GPCR signaling in these assays, despite the presence of a functional RBD in p110γ that can drive activation of recombinant p110γ in vitro (18). This result is consistent with work suggesting that receptor-independent activation of RAS by phorbol-esters in neutrophils [through RAS-GRP family RAS-guanine nucleotide exchange factors (29)] does not activate PI3Kγ (33).

The p110γ-Gβγ mutation resulted in defects in GPCR-stimulated PIP_3 formation, ROS production and motility in isolated neutrophils, and reduced neutrophil migration in thioglycolate-induced peritonitis and MIP-2-induced inflammation in ear pouch. These results show that direct interaction of Gβγ with p110γ is important for substantial activation of both p101/p110γ and p84/p110γ complexes (because of the reduction in both p101-dependent motility and p84-dependent ROS formation).

The p101-Gβγ mutation had variable effects in the assays used. There was no effect on fMLP-stimulated PIP_3 formation or motility in primary neutrophils but a reduction in MIP-2 or LTB4-simulated PIP_3 formation and also neutrophil migration in vivo. p101 plays an important role in fMLP-stimulated PIP_3 formation and in motility on fibrinogen (22, 27), and therefore, it is unexpected that this mutation did not have a bigger effect in these assays, particularly given it can substantially inhibit Gβγ activation of p101/p110γ in vitro(20). However, although the p101-Gβγ mutation alone had no impact on fMLP-stimulated PIP_3 formation, it reduced PIP_3 formation still further in combination with the p110γ-Gβγ mutation. This finding suggests that the organization of these signaling pathways at the endogenous level allows other mechanisms to compensate for loss of the p101-Gβγ interaction, for example through Gβγ binding to p110γ in either/both p101/p110γ or p84/p110γ, and/or through co-operation with GTP-RAS. The substantial increase in ROS formation in fMLP- and C5a-stimulated *p101*-Gβγ neutrophils suggests that loss of the p101-Gβγ interaction may promote increased activation of p84/p110γ, possibly through reduced competition for available Gβγ subunits, leading to relatively more p84/p110γ-driven PIP_3 and ROS formation and thus compensation for loss of p101-driven PIP_3-formation and increased overall ROS formation. Further, although not reaching statistical significance, we note the mean phosphorylation of ERK1/2 in the presence of the p101-Gβγ mutation was higher than in matched controls, and thus it is possible other Gβγ-effectors (such as RAS- or RAC-GEFs) may also be affected by reduced Gβγ-binding to p101. However, the manner in which the indirect effects of the loss of the Gβγ-p101 interaction play out within the complex signaling network engaged by Gi-coupled receptors is context specific, because although the fMLP- and C5a-induced ROS response was greater in *p101*-Gβγ neutrophils, the analogous responses to LTB4 and MIP-2 were either unaffected or reduced, respectively.

A comparison between *p110γ/p101*-dGβγ and *p110γ*-KO neutrophils for both fMLP-stimulated PIP_3 formation and ROS formation indicates loss of Gβγ interaction with both p101/p110γ and p84/p110γ complexes still leaves some residual GPCR-stimulated p110γ activity. The most plausible candidate for p110γ regulation under these circumstances is direct activation by GTPRAS, which has been shown previously to be important in these assays (27). However, comparison with the further reduced responses in *p84/p101*-dKO neutrophils suggests that, unlike in vitro, GTP-RAS interaction with p110γ in an

endogenous environment requires the presence of a regulatory subunit, perhaps suggesting a heterodimer is required for efficient targeting to a natural plasma membrane.

The results presented here begin to dissect the importance of direct regulation of p101/p110γ and p84/p110γ by Gβγ in a physiological context. Overall, and in the context of previous data characterizing the effect of direct GTP-RAS binding to p110γ (27), they suggest both p101/p110γ and p84/p110γ complexes are synergistically regulated by Gβγ and GTP-RAS. Our observation that the p101-Gβγ mutation had a larger effect on LTB4- and MIP-2-stimulated PIP_3 formation than the analogous *f*MLP-stimulated responses suggests there is differential coupling between GPCRs and p101/p110γ and p84/p110γ complexes. This could be because of receptor-specific differences in parallel signaling pathways (such as formation of GTP-RAS), quantitative or qualitative differences in Gβγ-signaling (for example, Gβγ subunit composition or location) or, some other reason (such as receptor-specific adaptors). In this respect, we note that the p101-Gβγ mutant still supports some activation of the p101/p110γ complex by higher Gβγ concentrations in vitro (20), and this weaker interaction with Gβγ may allow differential GPCR-derived Gβγ signals to be more clearly discerned in vivo. Unfortunately, we still lack a clear structural picture for how Gβγ activates a p101-p110γ complex and whether a single Gβγ site is modified by the presence of p101 or whether this regulatory subunit provides an additional Gβγ binding site. In either case, however, our data suggests the presence of p101 fine tunes the activation of p110γ by different Gβγ complexes. This issue will be important to resolve, because it may begin to explain how GPCRs with similar initial signal transduction machinery can elicit different physiological responses in the same target cells. We also still do not understand how p101/p110γ and p84/p110γ are coupled differentially to downstream effectors, for example ROS formation versus motility. Our initial attempts to isolate proteins that bind selectively to p84 or p101 resulted in the identification of 14-3-3 proteins which, based on our knowledge of how these proteins function in other systems, suggests a role in scaffolding signaling complexes. However, these proteins were found in both p84- and p101-based purifications. Some PI3Kγ-adaptor specific interactors were recovered in p84 and p101 pull downs from neutrophils, however, these results have not been validated by independent approaches and thus we still lack strong evidence indicating how p84- and p101-selective signaling may be organized in neutrophils.

Materials and Methods

Materials

*f*MLP, surfen, luminol, trimethylsilyl-diazomethane (TMS-diazomethane) in hexanes, fatty acid free bovine serum albumin (BSA) and horseradish peroxidase (HRP) were from Sigma-Aldrich. C5a was from R & D Systems, LTB4 from Enzo, and MIP-2 from PeproTech. All buffer components were from Sigma-Aldrich and were endotoxin free or low endotoxin, as available. Internal standards for lipid analysis, deuterated stereoyl arachidonyl 1-heptadecanoyl-2-hexadecanoyl-sn-glycero-3-(phosphoinositol-3,4,5-trisphosphate) (d6-C18:0/C20:4-PI(3,4,5)P_3), -(phosphoinositol-4,5-bisphosphate) (d6-C18:0/C20:4-PI(4,5)P_2), deuterated stereoyl arachidonyl – diacylglycerol (d6-C18:0/C20-4-DAG), and C17:0/C16:0-

PI as a hepta-sodium salt were synthesized at the Babraham Institute. All chemicals and solutions were analytical reagent grade.

Mouse strains

Rag2/IL2rg-deficient mice have been described previously (34). Mice lacking p110γ (*p110γ*-KO (6), p101 (*p101*-KO (27)) or p84 (*p84*-KO (22)), or expressing a point mutation in p110γ where the binding site for GTP-RAS is mutated (*p110γ*-RBD (27)) have been previously described. Mice with Gβγ-binding mutations in p101 (*p101*-Gβγ) or p110γ (*p110γ*-Gβγ), or lacking both p84 and p101 subunits (*p84/p101*-dKO) were created as described below. In all experiments, mice were compared with the most appropriate age and strain matched WT controls; thus *p101*-Gβγ, *p110γ*-Gβγ and *p110γ/p101*-dGβγ mice were compared to the same cohort of WT mice arising from the heterozygous crosses used to create these three strains; but *p84/p101*-dKO, *p110γ*-KO and *p110γ*-RBD mice were each compared to separate WT mice arising from independent breeding programs. Most of the results presented are values relative to the appropriate WT control, but for critical results the individual responses of the different WT strains are also presented in Supplementary Materials. Mice were housed in BSU at the Babraham Institute under specific pathogen-free conditions. All work was performed under Home Office Project license PPL P0302B91A.

Generation of *Pik3cg* ^{RK552DD} (*p110γ*-Gβγ) and *Pik3r5* ^{VVKR777AAAA} (*p101*-Gβγ) mice

The *Pik3cg* ^{RK552DD} and *Pik3r5* ^{VVKR777AAAA} targeting constructs were generated through recombineering methodology as previously described (35). This method uses the homologous recombination functions of the λ phage Red genes to subclone and retrieve DNA from bacterial artificial chromosomes into higher-copy plasmids and enables insertions, mutations, or deletions to be made in the retrieved gene of interest. *Pik3r5* was retrieved from PAC DNA containing approximately 30kb of *Pik3r5* genomic sequence as previously described (27), which was transferred into recombination-competent EL350 bacteria by electroporation, and resultant transformants selected with kanamycin (12.5μg/ml). The relevant *Pik3r5* fragment was retrieved by electroporating those transformants with 200 ng linearized and gel purified pBlueScript SK+ plasmid containing 5' and 3' *Pik3r5* homology retrieval arms. The 5' *Pik3r5* homology retrieval arm was generated with TGtcgacCGTTTCTGAACCCACTTACATCAT (forward primer) and GGgatatCAGAACTGGATGGGCTGGGATA (reverse primer). The 3' *Pik3r5* homology retrieval arm was generated with CTCTCgaTatcCCTCTTTCAGTAAAGTCCAAGTACAG (forward primer) and AGcggcCgCAGACTTGCTTGGAGCAGGAC (reverse primer). Lower case in these primers indicates mutated nucleotides. Both mini-homology arms were amplified from bacterial artificial chromosome DNA as a template, with the 5' homology arm flanked by the restriction sites SalI and EcoRV and the 3' arm flanked by EcoRV and EagI. Recombinants carrying the retrieved, gap-repaired *Pik3r5* portion in pBlueScript SK^+ were selected with ampicillin (100 μg/ml), conferred by the presence of the pBlueScript SK^+ backbone. Retrieval was confirmed by restriction digestion analysis of the isolated plasmid. Retrieved *Pik3cg* genomic DNA comprising of an 11.4-kb fragment, bracketed by XmnI sites, encompassing exons 1–4, was inserted into pGEM-T-easy vector as previously described (27). EL350 cells were electroporated with pBlueScript SK^+ containing the

retrieved *Pik3r5* fragment, or pGEMT-easy containing the retrieved *Pik3cg* fragment, for further modification, with successful transformants selected with100 μg/ml ampicillin.

Pik3r5 and *Pik3cg* genomic sequences in EL350 cells were further modified using a mini-targeting vector, based on vector PL452 which contains a neomycin cassette under the control of a prokaryotic (*em7*) and eukaryotic (*Pgk*) promoter flanked by two *loxP* sites, and had been previously further modified by the insertion of tACE-Cre to generate PL452-*loxP-tACE-CrePgk-em7-Neo-loxP* (36). Mini-targeting vectors were constructed by inserting 5' and 3' homology arms into PL452 to flank the *loxP-tACE-Cre-Pgk-em7-Neo-loxP* cassette. The 5' homology arm for *Pik3r5* was generated with GCgTcgacGAGGCAAGGTGGGGTACAAAT, (forward primer) and GAAGTTTGCAACGAaTTCAccCgggCATTAAAATAATTAAT (reverse primer). The 3' homology arm was generated with gcGgcCgcGATTTACATGGACTGCT (forward primer) and CAATGCACTGCCgtgTCCAACTCCGAGACCCC (reverse primer which included the insertion of SalI/EcoRI and NotI/AleI restriction sites respectively that were used to subclone the mini-homology arms into PL452, and subsequently for vector linearization). The 5' homology arm for *Pik3cg* was generated with GCTCGGATATTAGGTcGaCTACATCACTCAAACA (forward primer) and GAAGTTTGCAACGAaTTCAccCgggCATTAAAATAATTAAT (reverse primer). The 3' arm homology arm for *Pik3cg* was generated with gcGgcCgcGATTTACATGGACTGCT (forward primer) and GcacCTACgtgCATGAACATGTGGATAGT (reverse primer which introduced SalI/EcoRI and NotI/AleI restriction sites respectively).

Using two-step PCR, point mutations were introduced into the 5' mini-homology arm encompassing exon 2 of *Pik3cg* (5' primer, TGCCCAATCAGCTTgatgAtCAgTTGGAGGCGAT), resulting in amino acid exchange R552D and K553D and eliminating the MfeI restriction site. Two-step polymerase chain reaction (PCR) was also used to generate point mutations in the 3' mini-homology arm encompassing exon 17 of *Pik3r5* (5' primer, TAACCCTGACAGAgGccGcGgcGgccCAGAACCCTAAATC), resulting in amino acid exchange V777A, V778A, K779A, R800A and insertion of a BglI restriction site. To generate the final targeting vector, 200 ng of the linearized and gel purified mini-targeting construct (5' MHA-*loxP-tACE-Cre-Pgk-em7-Neo-loxP* −3'MHA) was electroporated into EL350 cells carrying the retrieved genomic DNA. Transformed EL350 cells were selected for em7-neo expression with 12.5 μg/ml kanamycin and the plasmids further screened by restriction digests. To ensure purity of the final targeting vectors, extracted DNAs were digested, religated, and transformed into DH5α cells and transformants were selected with kanamycin (12.5 μg/ml). Diagnostic digests confirmed the final targeting vector was as designed. Excision of the *loxP-tACE-Cre-Pgk-em7-Neo-loxP* cassette was confirmed by loss of kanamycin resistance in arabinose-induced EL350 cells, and the resulting plasmids were checked by restriction digests. Finally, both *Pik3cg* ^{RK552DD} and *Pik3r5* ^{VVKR777AAAA} targeting vectors were fully sequenced.

Linearized final targeting vectors were electroporated into E14 129/Ola ES cells by the Gene Targeting Facility at the Babraham Institute. Neomycin resistant clones were picked and screened by PCR for homologous recombination, and the positive clones were expanded and

screened by Southern blot using 5' and 3' probes. The *Pik3r5* 5' probe consisted of CAGAGTGGGGGTTAGCACAGAGAA (forward primer) and CAACAAAAGTGTGAGCCTGACTTTTC (reverse primer). The *Pik3r5* 3' probe consisted of GGAGGTGGGTGGGGCTAGACA (forward primer) and ACCCGCCTTCTCCTGCCCA (reverse primer). The *Pik3cg* 5' probe consisted of ACAAGGACTGTGTGAGAGGAAATAGAA (forward primer) and GCCTGGGAACTCACTTCCTTACATTG (reverse primer). The *Pik3cg* 3' probe consisted of TTTAGCAATATTTTCACTAGACAGAGAATCC (forward primer) and TGTCTGAAATATTATTACTACAGAACCCAA (reverse primer). Examples of Southern analysis can be found in figures S3B (*Pik3r5*) and figure S2B (*Pik3cg*).

Two clones each for *Pik3cg* and *Pik3r5* were taken forward for blastocyst injection (C57BL/6) and resulting chimeras were bred with each other to generate a mixed C57BL/6 129/Ola genetic background. The *Pik3cg* ^{RK552DD} and *Pik3r5* ^{VVKR777AAAA} mice were viable, born at expected Mendelian ratios, of normal size and had normal blood counts (table S1).

To confirm the presence of the correct Pik3cgRK55DD mutation, RT-PCR analysis was performed on mouse biopsies using forward (AGAAGAGGTACTCTGGAATGTGTGG) and reverse (CTAACCAGCAGCCCCTACCTGTAC) primers to generate a 793-bp fragment. Cleavage of the fragment with MfeI generated 343- and 450-bp fragments with WT DNA, whereas the fragment containing the RK552DD mutation remained intact as a result of removal of the MfeI site in the targeted sequence (fig. S2C).

To confirm the presence of the Pik3rVVKR777AAAA mutation, RT-PCR analysis was performed on mouse biopsies using CTGAGCCCTCCTCACCAGAGC (forward primer) and CTAACCAGCAGCCCCTACCTGTAC (reverse primer) to generate a 1113-bp fragment. Cleavage with BglI was predicted to leave the WT fragment intact, whereas 374- and 739-bp fragments were generated in targeted sequences through a site introduced by the VVKR777AAAA mutation (fig. S3, C). Mice expressing point mutations of both genes (*p110γ/p101*-dGβγ) were generated by cross-breeding of *p101*-Gβγ and *p110γ*-Gβγ lines.

Generation of *p84/p101*-dKO mice

Mice lines lacking both p84 and p101 (*p84/p101-dKO*) were generated by genOway Genome Engineering by sequential targeting of *Pik3r5* (p101) and *Pik3r6* (p84) in E14Tg2a (E14) ES cells derived from the 129P2/OlaHsd (129Ola) mouse strain. Because *Pik3r5* and *Pik3r6* are neighbouring genes, attempting to derive *p84* $^{-/-}$ x *p101* $^{-/-}$ mice by traditional crossing of *p84* $^{-/-}$ and *p101* $^{-/-}$ strains would create those mice at extremely low frequency.

The p101 BB12A-HR targeting vector is shown in fig. S1A. A clone in which most of exon 2 and all of exons 3 and 4 were disrupted by in-frame insertion of a β-galactosidase/ neomycin cassette was identified by PCR-mediated diagnostic analysis and then subjected to a p84-targeting strategy.

Targeting of p84 also used the pBB12A-HR targeting vector (fig. S1C) to create a LoxP-flanked 625bp fragment containing exon 4 and parts of the surrounding intronic regions.

Cre-mediated deletion of the fragment resulted in a frame-shift and disrupted expression of p84.

To identify ES cells double targeted in cis (in which both p101 and p84 had been disrupted on the same chromosome), a panel of double recombinant targeted ES cells were injected into blastocytes to generate chimeras. The resulting chimeras were then bred with WT (C57BL/6) mice and their progeny screened for both mutations. Heterozygous mice carrying both mutations were identified (and confirmed by southern screening) and transferred to the Babraham Institute BSU facility for inter-breeding, with double KOs identified and confirmed by PCR analysis (see below) and immunoblotting for p101 and p84 (Fig. 1B).

Genotyping of p101 from biopsy-extracted cDNA required two separate PCR reactions on each sample to identify WT or KO sequence. Both reactions employed the same forward primer (GATAAACCTTCCGGAAGCTG) in conjunction with specific reverse primers for WT (GAACCTGCTTCTAGTCATTCG) or *p101*-KO (CGGATTGACCGTAATGGGATAG, which amplified across the β-GAL sequence). Such primers were used to amplify fragments of 570-bp (fig. S1D) in WT and KO reactions. Identification of *p84*-KO was performed using forward primer (5'-GGACCTAGAATCATTCAGAA-3') and a reverse primer (5'-CATGGATAAGTTCAGGTGG-3') to amplify a WT 718-bp fragment and a knockout 621-bp fragment. (fig. S1C).

Preparation of Neutrophils

For ROS assays and lipid/DAG analysis, mature mouse neutrophils were isolated from bone marrow at room temperature on a discontinuous Percoll+ gradient as described previously (37). Purity was determined by cytospin and REASTAIN Quick-Diff (Reagena) staining, and was between 75-90% neutrophils. After washing, neutrophils were resuspended in Dulbecco's phosphate buffered saline (PBS) with Ca^{2+} and Mg^{2+}, 1g/l glucose, 4mM sodium bicarbonate (dPBS+) at a concentration of $6.25x10^6$/ml (ROS assays), $7.4x10^6$/ml (lipid assays) or $3.3x10^6$/ml (DAG assay).

Western blot analysis

Neutrophils ($1x10^6$, Fig. 1; $0.5x10^6$, fig. S5) prepared at room temperature as described above were resuspended in SDS loading buffer and freeze-thawed and sonicated. Samples were resolved using SDS-polyacrylamide gel electrophoresis (SDS-PAGE) at 150V and transferred overnight at 35V. For quantification of PI3Kγ subunits, they were immunoblotted with either rabbit α-p101 (Cell Signaling), rabbit α-p84 ((27)), rabbit α-p110γ and $p67^{phox}$ (Millipore), or mouse α-βcop (a kind gift from N. Ktistakis, Babraham Institute). For p42/44 ERK and PKB activation, bone marrow neutrophils (BMNs) were incubated for 3 min at 37°C prior to fMLP stimulation (or vehicle) for 1 min and stopped with cold PBS. Cell lysates were immunoblotted for P-PKB–Ser^{473} (Cell Signaling, 1:2500), P-42/44 ERK (Cell Signaling, 1:1000), PKB (Cell Signalling, 1:1000), ERK (Cell Signalling, 1:1000), βcop (gift from N. Ktistakis, 1:250), $p47^{phox}$ (Upstate, 1:4000) and $p67^{phox}$ (Millipore, 1:2000). Signal was detected by ECL and bands were quantified by using ImageJ or Image Studio Lite. Where indicated, anti-$p67^{phox}$ was used as a loading

control to normalize for neutrophil input between different bone marrow derived neutrophil preparations.

Lipid Analysis

For lipid measurements, we modified the method previously described by Clark et al (38) to enrich the lipid extract for polyphosphoinositides prior to derivatisation and mass spectrometry; this improved the signal/noise ratio for low PIP_3 signals in our neutrophil extracts. Neutrophils ($1x10^6$) in 135 µl were added to 865 µl dPBS+ (pre-warmed at 37°C for 90 sec) containing agonist at indicated concentrations (fMLP, MIP-2, LTB4, C5a or surfen), and incubated at 37°C for indicated times. Reactions were terminated by addition of 5-ml initial organic mix ($CHCl_3$: MeOH 1:2 v:v) and thorough mixing to form a single phase. Samples were then either stored at −80°C overnight, or lipids extracted immediately. Internal standards d6-C18:0/C20:4-PIP_3 (10 ng) and –$PI(4,5)P_2$ (100 ng) were added to initial extract suspensions. Samples were washed twice with 4.5 ml $CHCl_3$ and the resulting lower phase discarded each time (the addition of $CHCl_3$ forms a neutral two-phase system in which the polyphosphoinositides are found in the upper phase and non-polar lipids in the lower phase). The upper phase was then loaded onto a 1ml Sep-Pak aminopropyl anion-exchange cartridge (Waters WAT023610, 100-mg sorbent) that had been pre-equilibrated with 3x 1ml initial organic mix : H_2O [725:170(v/v)]. Samples were passed through the column under low vacuum on a manifold, and unbound material removed by 2x -ml washes with initial organic mix: H_2O. Low binding components were eluted with 2x 1ml washes of column wash buffer {0.5M CH_3COONH_4, made up in $CHCl_3$: MeOH : H_2O [10:9:1 (v:v:v)]}, followed by washing with 3x1ml initial organic mix:H_2O. PIP_3 and PIP_2 were eluted with 1-ml acid elution buffer {$CHCl_3$: MeOH : 10 M HCl [1:2:0.124 (v:v:v)]} followed by 700 µl $CHCl_3$. Phases were then split by the addition of 340 µl of H_2O and the lower phase of the now acidified two phase system was removed and the lipids within it were derivatized with trimethylsilyldiazomethane and analyzed by mass spectrometry as previously described (38), except that an additional pre-derivitization wash was included and the final samples were resuspended in 50µl MeOH : H_2O 4:1 v:v. C38:4-PIP_3 and -PIP_2, the major acyl-chain species of neutrophil inositol phospholipids (38)were measured by mass spectrometry, employing neutral loss of derivitized head groups, using a ABSciex QTRAP4000 connected to a Waters Acquity UPLC system as described in Clark et al (38). Data are shown as response ratios, calculated by normalizing the multiple reaction monitoring (MRM) -targeted lipid integrated response area to that of a known amount of relevant internal standard. PIP_3 response ratios were normalized to PIP_2 response ratio to account for any cell input variability.

C18:0 C20:4 (S/A)-DAG levels in $0.5x10^6$ BMN were measured in response to 1 min *f*MLP (10 µM final) as previously described (29) with the addition of 10 ng C16:0/C17:0-PI ISD added to samples prior to extraction. Data shown are response ratios of DAG normalized to PI response ratios from the same sample to account for cell input variability.

Measurement of ROS production

Rate kinetics of ROS production was measured by chemiluminescence using a luminol-based assay in polystyrene 96-well plates (Berthold Technologies), as described previously

(39). Briefly, neutrophils (0.5×10^6) were incubated with luminol (150 μM) and HRP (18.75 U/ml) for 5 min at 37°C before being added manually to wells containing *f*MLP (10 μM final), or PMA (1 μM final). Measurements were started immediately and light emission was recorded by a Berthold Mircolumat Plus luminomter (Berthold Technologies). Measurements of MIP-2-, LTB4- and C5a-induced ROS responses were performed by adding agonists through the luminometer injection port to the neutrophil/HRP/luminol mix (at 1), employing previously described methods(37). Data output was in relative light units (RLUs) per second or total RLUs integrated over 80 s (*f*MLP), 5 min (PMA), 25 s (MIP-2, LTB4), or 75 seconds (C5a) after injection. Where indicated, data are expressed as a percentage of the matched WT superoxide response. RLUs measured in control PBS injections were subtracted from MIP-2 ROS responses for each experiment.

EZ-Taxiscan Migration

The EZ-Taxiscan chamber migration studies were performed essentially as described previously (30) with the following modifications to neutrophil preparation. Mouse bone marrow cells in Hanks' balanced salt solution (HBSS) were overlaid on 56% Percoll and centrifuged at 1639*g* for 30 min at 4°C. Neutrophils within the Percoll layer were collected and washed twice, and the red blood cells were lysed and resuspended at $3x10^5$ cells/ml in assay buffer (HBSS, 15mM Hepes, 0.05% fatty acid-free BSA, 1 mM $CaCl_2$, 0.5 mM $MgCl_2$). One microliter of cell suspension was loaded into the EZ-Taxiscan chamber (Effector Cell Institute, Tokyo, Japan), 1μl of 3μM *f*MLP added and cell migration was recorded every 30 s for 30 min using a 10× objective on a Olympus CellR maintained at 37 °C in a humidified environmental chamber. Glass coverslips used in the chamber were washed thoroughly in changes of acid, water and ethanol, prior to coating with fibrinogen (2.5mg/ml) for 1 hour at 37°C.

In vivo neutrophil migration assay: Thioglycollate-induced peritonitis

Mice were injected intraperitoneally with 200 μl 3% thioglycolate medium, killed after 3.5 hours and their peritonea washed with 9 ml PBS, 5 mM EDTA. The recovered cells were resuspended in 0.2 ml HBSS, 5 mM EDTA and stained for 1 hour at 4°C for flow cytometry [antibodies used were CD11b-PE (M1/70, eBioscience), Ly6G BV510 (1A8 BD Biosciences), Ly6C-BV605 (AL-21, BD Biosciences), F4/80 BV711 (T45-2342 BD Biosciences), CD4 BV786 (RM4-5 BD Biosciences), CD8-APCCy7 (53-6.7 BD Biosciences), CD19-PE-Cy7 (1D3 BD Biosciences), CD45-PerCP-Cy5.5 (30-F11, BD Biosciences)].

In vivo neutrophil migration assay: Inflammation of ear pinnae

Analysis of in vivo neutrophil infiltration in ear inflammation was performed essentially as described previously(40). Mice were anaesthetized under isoflurane and approximately 10 μl of 1.5 μM MIP-2 (Peprotech) or PBS was intradermally injected into the pinnae until a blister of 5mm diameter was formed. Pinnae were collected after 4 hours, fixed for 20 min in ice cold 4% paraformaldehyde (PFA), blocked and permeabilised with PBS, 5% BSA, 0.5% Triton X-100 for 3 hours at room temperature and washed three times with PBS. Tissues were stained overnight at 4°C with Ly6G-PE (1A8, Biolegend), CD11b-eFluor660 (M1/70, eBioscience) and VEcadherin-Alexa Fluor 488 (eBioBV13, eBioscience), washed in PBS

for 1.5 hours, and compressed between two coverslips for imaging. Neutrophil infiltration was imaged using a 20x multi-immersion objective on a Nikon A1R, with at least 10 fields of view taken per pinna and analysed using ImageJ.

Generation of retroviral vectors

The retroviral transfer vector pMIGR1, in which the internal ribosomal entry site sequence has been removed, has been previously described (41). Full length p84 cDNA was amplified with primers inserting SacII and NotI restriction sites (forward primer TTCCCCGCGGATGGAGAGCTCAGATGTGGAG; reverse primer TTTTCCTTTTGCGGCCGCTTATTGGATTATGCCAGAGAATG) and subcloned into pHTN HaloTag CMV-neo (Promega). A HaloTag p84 PCR product was then generated with a 5' HpaI restriction site (forward primer AATTAAAATGTTAACATGGCAGAAATCGGTACTG), digested with HpaI and NotI and subcloned into pMIGR1. Full length p101 cDNA was amplified with primers inserting 5' and 3' EagI restriction sites (forward primer GATACGGCCGAGGCATGCAGCCAGCAGCCACAAC, reverse primer AACGCGGCCGCCTAGGGCAGAG) and subcloned into pMIGR1-GFP. Both pMIGR1-HaloTag p84 and pMIGR1-GFP p101 were sequenced to confirm the correct orientation and absence of mutations.

Production of retroviral vectors

HALO-p84 and GFP-p101 retroviral supernatants were generated in Plat-E cells, using previously described methods (41). Briefly, 1.2 x10^7 Plat-E cells plated in 14-cm tissue culture plates were transiently transfected with 16.8 μg pMIGR1-HaloTag-p84 or pMIGR1-GFP-p101 and 50.4 μl Lipofectamine 2000 in Optimem. Twenty-four hours after transfection, the medium containing DNA-Lipofectamine complexes was replaced by StemPro34 serum-free medium supplemented with 1% antibiotic/antimycotic, and 48 hours after transfection the viral supernatant was harvested and centrifuged at 800*g* for 5 min to pellet debris and filtered through a 0.45-μm filter.

Generation of neutrophils retrovirally expressing HALO-p84 and GFP-p101

Fully differentiated *p84*-KO and *p101*-KO neutrophils retrovirally expressing HALO-p84 and GFP-p101 respectively were generated using a previously described method (42). Briefly, fetal liver cells from 13.5-day-old *p84*-KO and *p101*-KO mouse embryos were harvested, cultured for 24 hours in Stempro-34 medium supplemented with 1% antibiotic and antimycotic, 1% glutamax, and cytokines [mSCF (100 ng/ml), thrombopoietin (TPO) (100 ng/ml), interleukin-6 (IL-6) (10 ng/ml), IL-3 (6 ng/ml), and Flt3L (20ng/ml)], and transduced overnight with filtered retroviral supernatant in retronectin-coated wells at 5x10^5 cells/ml. Transduced fetal liver cells expressing HALO-p84 or GFP-p101 were washed in PBS and resuspended in PBS with 10% Ffetal bovine serum to a concentration of 5x10^6 cells/ml, and a volume of up to 300μl (and not exceeding 1% v/w of the mouse) was injected using an 27-gauge needle into the tail vein of a *Rag2/IL2rg*-deficient mouse irradiated 24 hours earlier with two doses of 500 rads, 3 hours apart. Mice were given drinking water supplemented with neomycin (80mg/ml) for 4 weeks starting on the day of irradiation. Efficiency of haematopoietic cell transfer and percentage of neutrophils expressing HALO-

Europe PMC Funders Author Manuscripts

p84 or GFP-p101 was determined with tail vein bleeds by flow cytometry 6 weeks after transfer. Mice were sacrificed, and neutrophils isolated from bone marrow for experiments at 8 to12 weeks post transfer.

HALO-p84 and GFP-p101 pull downs

For pull downs, isolated neutrophils were treated with diisofluorophosphate (DFP) 1:1000 for 5 min at RT (all safety procedures regarding the use of DFP were followed, and all solutions containing DFP were neutralised in concentrated NaOH), washed with PBS and resuspended at 5 x 10^7 cells/ml in PBS. Cells were warmed at 37°C for 3 min, stimulated with *f*MLP (10 μm, 10 s) or vehicle, and stimulation was terminated by transferring the samples to ice and incubating for 10 min with ice cold PFA (final concentration 0.75% PFA; cross-linking) or Hepes (native). PFA was neutralized with 125 mM glycine for 2 min on ice, and agitated on ice for 10 min with lysis buffer (final lysis buffer composition of 20 mM Hepes (pH 8.0), 100 mM NaCl, 1 mM EGTA, 1 mM MgCl2, detergent [0.3% n-dodecyl beta-D-maltoside (DDM) for HALO-p84; 0.5% NP-40 for GFP-p101], protease inhibitors (0.1 mM phenylmethylsulfonyl fluoride, and aprotinin, leupeptin, antipain and pepstatin A (10 μg/ml each), and phosphatase inhibitors [1 mM β-glycerophosphate and 0.1 mM sodium orthovanadate]). Samples were sonicated briefly on ice and centrifuged at 16,000*g* for 15 min at 4°C. Supernatants were applied to pre-equilibrated HaloLink resin (Promega) or GFP-Trap MA beads (Chromotek) and tumbled end-over-end at 4°C for 5 to 6 hours, or 1 hour, respectively. The resin and beads were washed four times, resuspended in Laemmli buffer and heated at 95°C for 30 min. Samples were stored at −20°C until processing for mass spectrometric proteomic analysis described below.

For analysis of pull-down efficiency (fig. S8, A to D), aliquots of samples were collected prior to (Pre) and following (Post) incubation with HaloLink resin or GFP-trap MA beads as relevant. Samples were subjected to SDS-PAGE and blotted for HALO-p84 (rabbit α-Halo, Promega) or pGFP-101 (mouse α-GFP, Roche) as indicated.

Proteomic Analysis

Immunoprecipitated proteins were run ~5mm into an SDS-PAGE gel then stained with Coomassie. Protein-containing gel regions were excised, de-stained, reduced, alkylated and trypsin digested as previously described (43). The resulting peptides were separated on a reversed-phase column (0.075 mm by 150 mm, Reprosil-Pur C18AQ, 3-μm particles) with a 60-min linear gradient from 0 to 35% acetonitrile (containing 0.1% formic acid) at a flow rate of 300 nl/min with a Proxeon nanoHPLC. The column was interfaced to a Thermo Scientific Orbitrap Velos Pro mass spectrometer operating in data-dependent mode, with an acquisition cycle of one high-resolution MS1 scan followed by low-resolution ion-trap MS2 scans of the 20 most abundant precursor ions. Mass spectral data were analysed using ProgenesisQI software for quantitative analysis, and Mascot for database searching.

Statistics

Data shown are mean ± SEM for at least three experiments (unless otherwise indicated). With the exception of Western blot protein quantitation (Fig. 1B and Fig. 2, F to H) and superoxide assays with HALO-p84 (fig. S8B) where ratio paired *t* tests were performed with

Holms-Sidak corrections applied to account for multiple comparisons, all statistics were performed on non-normalized data using the methods outlined below. When data showed log-normal distribution they were log-transformed to meet the assumption for parametric tests. For PIP_3 time course assays (Fig. 2, B and E) and superoxide responses (Fig. 3, B to F) areas under the curve from each genotype response were compared to its relevant WT in the same experiment using a series of ratio paired *t* tests, whereas a one-way ANOVA, on log-transformed data, was used for comparisons between genotypes. Holm-Sidak correction was applied to account for multiple comparisons. A 2-way ANOVA on nontransformed (Fig 2G, DAG analysis) or log transformed data (Fig 2C, comparison of PIP_3 responses to multiple agonists) followed by Sidak's multiple comparison test were used. For ERK and PKB Western (Fig 2, F and H), one sample Student *t* tests followed by Holm-Sidak corrections were performed to compare genotypes to WT in the presence of *f*MLP. A *t* test was used to compare surfen PIP_3 data (Fig. 2D). A one-way ANOVA followed by Dunnett's multiple comparison tests were performed for analysis of EZ-taxiscan (Fig. 4B) and, peritonitis and ear inflammation data (Fig. 4C and D, fig. S7, A and B).

Supplementary Material

Refer to Web version on PubMed Central for supplementary material.

Acknowledgments

We would like to thank members of the Small Animal Breeding Unit at the Babraham Institute for animal husbandry; A. Segonds-Pichon for statistical analysis; I. Niewczas and K. Davidson for technical assistance, and T. Chessa for critical reading of the manuscript.

Funding

This work was supported by funding from the Biotechnology and Biological Sciences Research Council (BBSRC) UK (BB/J004456/1 and BB/P013384/1 supporting K.E.A., S.S., L.R.S., and P.T.H.; PI on award L.R.S.) and the Medical Research Council MRC (MR/K018167/1 supporting N.K.R and E.K.; PI on award L.R.S.), D.M.C. is a recipient of an Amgen Scholars Programme Award. O.V. was supported by a Swiss National Science Foundation fellowship (grant PA00P3_134202) and a European Commission fellowship (FP7-PEOPLE-2010-IEF, N°275880).

Data and materials availability

Proteomic data have been deposited in the PRIDE-proteomics Identification Database with the submission reference 1-20200729-134222. All other data needed to evaluate the conclusions in the paper are present in the paper or the Supplementary Materials. Use of the *p101/p84*-dKO, *p110γ*-Gβγ, *p101*-Gβγ and *p110γ/p101*-dGβγ mice requires a material transfer agreement from the Babraham Institute.

References and notes

1. Fruman DA, Chiu H, Hopkins BD, Bagrodia S, Cantley LC, Abraham RT. The PI3K Pathway in Human Disease. Cell. 2017; 170:605–635. [PubMed: 28802037]
2. Nürnberg B, Beer-Hammer S. Function, Regulation and Biological Roles of PI3Kγ Variants. Biomolecules. 2019; 9:427.
3. Stephens LR, Hughes KT, Irvine RF. Pathway of phosphatidylinositol(3,4,5)-trisphosphate synthesis in activated neutrophils. Nature. 1991; 351:33–39. [PubMed: 1851250]

4. Stephens LR, Eguinoa A, Erdjument-Bromage H, Lui M, Cooke F, Coadwell J, Smrcka AS, Thelen M, Cadwallader K, Tempst P, Hawkins PT. The G beta gamma sensitivity of a PI3K is dependent upon a tightly associated adaptor, p101. Cell. 1997; 89:105–114. [PubMed: 9094719]
5. Li Z, Jiang H, Xie W, Zhang Z, Smrcka AV, Wu D. Roles of PLC-beta2 and -beta3 and PI3Kgamma in chemoattractant-mediated signal transduction. Science. 2000; 287:1046–1049. [PubMed: 10669417]
6. Hirsch E, Katanaev VL, Garlanda C, Azzolino O, Pirola L, Silengo L, Sozzani S, Mantovani A, Altruda F, Wymann MP. Central role for G protein-coupled phosphoinositide 3-kinase gamma in inflammation. Science. 2000; 287:1049–1053. [PubMed: 10669418]
7. Sasaki T, Irie-Sasaki J, Jones RG, Oliveira-Dos-Santos AJ, Stanford WL, Bolon B, Wakeham A, Itie A, Bouchard D, Kozieradzki I, Joza N, et al. Function of PI3Kgamma in thymocyte development, T cell activation, and neutrophil migration. Science. 2000; 287:1040–1046. [PubMed: 10669416]
8. Suire S, Coadwell J, Ferguson GJ, Davidson K, Hawkins P, Stephens L. p84, a new Gbetagamma-activated regulatory subunit of the type IB phosphoinositide 3-kinase p110gamma. Curr Biol. 2005; 15:566–570. [PubMed: 15797027]
9. Voigt P, Dorner MB, Schaefer M. Characterization of p87PIKAP, a novel regulatory subunit of phosphoinositide 3-kinase gamma that is highly expressed in heart and interacts with PDE3B. Journal of Biological Chemistry. 2006; 281:9977–9986.
10. Shymanets A, Prajwal, Bucher K, Beer-Hammer S, Harteneck C, Nürnberg B. p87 and p101 subunits are distinct regulators determining class IB phosphoinositide 3-kinase (PI3K) specificity. J Biol Chem. 2013; 288:31059–31068. [PubMed: 24014027]
11. Rückle T, Schwarz MK, Rommel C. PI3Kγ inhibition: towards an ‘aspirin of the 21st century’? Nat Rev Drug Discov. 2006; 5:903–918. [PubMed: 17080027]
12. Hawkins PT, Stephens LR. PI3K signalling in inflammation, Biochim. Biophys Acta. 2015; 1851:882–897.
13. Wymann MP, Solinas G. Inhibition of phosphoinositide 3-kinase γ attenuates inflammation, obesity, and cardiovascular risk factors. Ann NY Acad Sci. 2013; 1280:44–47. [PubMed: 23551103]
14. Kaneda MM, Messer KS, Ralainirina N, Li H, Leem C, Gorjestani S, Woo G, Nguyen AV, Figueiredo CC, Foubert P, Schmid MC, et al. PI3Kγ is a molecular switch that controls immune suppression. Nature. 2016; 539:437–442. [PubMed: 27642729]
15. De Henau O, Rausch M, Winkler D, Campesato LF, Liu C, Cymerman DH, Budhu S, Ghosh A, Pink M, Tchaicha J, Douglas M, et al. Overcoming resistance to checkpoint blockade therapy by targeting PI3Kγ in myeloid cells. Nature. 2016; 539:1–16.
16. Gangadhara G, Dahl G, Bohnacker T, Rae R, Gunnarsson J, Blaho S, Öster L, Lindmark H, Karabelas K, Pemberton N, Tyrchan C, et al. A class of highly selective inhibitors bind to an active state of PI3Kγ. Nat Chem Biol. 2019; 15:348–357. [PubMed: 30718815]
17. Luo L, Wall AA, Tong SJ, Hung Y, Xiao Z, Tarique AA, Sly PD, Fantino E, Marzolo M-P, Stow JL. TLR Crosstalk Activates LRP1 to Recruit Rab8a and PI3Kγ for Suppression of Inflammatory Responses. CellReports. 2018; 24:3033–3044.
18. Suire S, Hawkins P, Stephens L. Activation of phosphoinositide 3-kinase gamma by Ras. Curr Biol. 2002; 12:1068–1075. [PubMed: 12121613]
19. Pacold ME, Suire S, Perisic O, Lara-Gonzalez S, Davis CT, Walker EH, Hawkins PT, Stephens L, Eccleston JF, Williams RL. Crystal structure and functional analysis of Ras binding to its effector phosphoinositide 3-kinase gamma. Cell. 2000; 103:931–943. [PubMed: 11136978]
20. Vadas, O; Dbouk, HA; Shymanets, A; Perisic, O; Burke, JE; Abi Saab, WF; Khalil, BD; Harteneck, C; Bresnick, AR; Nürnberg, B; Backer, JM; , et al. Molecular determinants of PI3Kγ-mediated activation downstream of G-protein-coupled receptors (GPCRs). Proceedings of the National Academy of Sciences of the United States of America; 2013. 18862–18867.
21. Kurig B, Shymanets A, Bohnacker T, Prajwal, Brock C, Ahmadian MR, Schaefer M, Gohla A, Harteneck C, Wymann MP, Jeanclos E, et al. Ras is an indispensable coregulator of the class IB phosphoinositide 3-kinase p87/p110γ. Proc Natl Acad Sci USA. 2009; 106:20312–20317. [PubMed: 19906996]

22. Deladeriere A, Gambardella L, Pan D, Anderson KE, Hawkins PT, Stephens LR. The regulatory subunits of PI3Kγ control distinct neutrophil responses. Sci Signal. 2015; 8:ra8–ra8. [PubMed: 25605974]
23. Bohnacker T, Marone R, Collmann E, Calvez R, Hirsch E, Wymann MP. PI3Kgamma adaptor subunits define coupling to degranulation and cell motility by distinct PtdIns(3,4,5)P3 pools in mast cells. Sci Signal. 2009; 2:ra27–ra27. [PubMed: 19509406]
24. Schmid MC, Avraamides CJ, Dippold HC, Franco I, Foubert P, Ellies LG, Acevedo LM, Manglicmot JRE, Song X, Wrasidlo W, Blair SL, et al. Receptor tyrosine kinases and TLR/IL1Rs unexpectedly activate myeloid cell PI3kγ, a single convergent point promoting tumor inflammation and progression. Cancer Cell. 2011; 19:715–727. [PubMed: 21665146]
25. Brazzatti JA, Klingler-Hoffmann M, Haylock-Jacobs S, Harata-Lee Y, Niu M, Higgins MD, Kochetkova M, Hoffmann P, McColl SR. Differential roles for the p101 and p84 regulatory subunits of PI3Kγ in tumor growth and metastasis. Oncogene. 2011; 31:2350–2361. [PubMed: 21996737]
26. Perino A, Ghigo A, Ferrero E, Morello F, Santulli G, Baillie GS, Damilano F, Dunlop AJ, Pawson C, Walser R, Levi R, et al. Integrating cardiac PIP3 and cAMP signaling through a PKA anchoring function of p110γ. Mol Cell. 2011; 42:84–95. [PubMed: 21474070]
27. Suire S, Condliffe AM, Ferguson GJ, Ellson CD, Guillou H, Davidson K, Welch H, Coadwell J, Turner M, Chilvers ER, Hawkins PT, et al. Gbetagammas and the Ras binding domain of p110gamma are both important regulators of PI(3)Kgamma signalling in neutrophils. Nat Cell Biol. 2006; 8:1303–1309. [PubMed: 17041586]
28. Surve CR, To JY, Malik S, Kim M, Smrcka AV. Dynamic regulation of neutrophil polarity and migration by the heterotrimeric G protein subunits Gαi-GTP and Gβγ. Sci Signal. 2016; 9:ra22–ra22. [PubMed: 26905427]
29. Suire S, Lecureuil C, Anderson KE, Damoulakis G, Niewczas I, Davidson K, Guillou H, Pan D, Clark Jonathan, Hawkins Phillip T, Stephens L. GPCR activation of Ras and PI3Kc in neutrophils depends on PLCb2/b3 and the RasGEF RasGRP4. EMBO J. 2012; 31:3118–3129. [PubMed: 22728827]
30. Ferguson GJ, Milne L, Kulkarni S, Sasaki T, Walker S, Andrews S, Crabbe T, Finan P, Jones G, Jackson S, Camps M, et al. PI(3)Kgamma has an important context-dependent role in neutrophil chemokinesis. Nat Cell Biol. 2007; 9:86–91. [PubMed: 17173040]
31. Walser R, Burke JE, Gogvadze E, Bohnacker T, Zhang X, Hess D, Küenzi P, Leitges M, Hirsch E, Williams RL, Laffargue M, et al.PKCβ phosphorylates PI3Kγ to activate it and release it from GPCR control. PLoS Biol. 2013; 11
32. Gardino AK, Yaffe MB. 14-3-3 proteins as signaling integration points for cell cycle control and apoptosis. Seminars in Cell and Developmental Biology. 2011; 22:688–695. [PubMed: 21945648]
33. Stephens L, Eguinoa A, Corey S, Jackson T, Hawkins PT. Receptor stimulated accumulation of phosphatidylinositol (3,4,5)-trisphosphate by G-protein mediated pathways in human myeloid derived cells. EMBO J. 1993; 12:2265–2273. [PubMed: 8389691]
34. Colucci F, Soudais C, Rosmaraki E, Vanes L, Tybulewicz VL, Di Santo JP. Dissecting NK cell development using a novel alymphoid mouse model: investigating the role of the c-abl proto-oncogene in murine NK cell differentiation. J Immunol. 1999; 162:2761–2765. [PubMed: 10072522]
35. Liu P, Jenkins NA, Copeland NG. A highly efficient recombineering-based method for generating conditional knockout mutations. Genome Res. 2003; 13:476–484. [PubMed: 12618378]
36. Houslay DM, Anderson KE, Chessa T, Kulkarni S, Fritsch R, Downward J, Backer JM, Stephens LR, Hawkins PT. Coincident signals from GPCRs and receptor tyrosine kinases are uniquely transduced by PI3Kβ in myeloid cells. Sci Signal. 2016; 9:ra82–ra82. [PubMed: 27531651]
37. Condliffe AM, Davidson K, Anderson KE, Ellson CD, Crabbe T, Okkenhaug K, Vanhaesebroeck B, Turner M, Webb L, Wymann MP, Hirsch E, et al. Sequential activation of class IB and class IA PI3K is important for the primed respiratory burst of human but not murine neutrophils. Blood. 2005; 106:1432–1440. [PubMed: 15878979]

38. Clark J, Anderson KE, Juvin V, Smith TS, Karpe F, Wakelam MJO, Stephens LR, Hawkins PT. Quantification of PtdInsP3 molecular species in cells and tissues by mass spectrometry. Nat Methods. 2011; 8:267–272. [PubMed: 21278744]

39. Anderson KE, Boyle KB, Davidson K, Chessa TAM, Kulkarni S, Jarvis GE, Sindrilaru A, Scharffetter-Kochanek K, Rausch O, Stephens LR, Hawkins PT. CD18-dependent activation of the neutrophil NADPH oxidase during phagocytosis of Escherichia coli or Staphylococcus aureus is regulated by class III but not class I or II PI3Ks. Blood. 2008; 112:5202–5211. [PubMed: 18755982]

40. Colom B, Bodkin JV, Beyrau M, Woodfin A, Ody C, Rourke C, Chavakis T, Brohi K, Imhof BA, Nourshargh S. Leukotriene B4-Neutrophil Elastase Axis Drives Neutrophil Reverse Transendothelial Cell Migration In Vivo. Immunity. 2015; 42:1075–1086. [PubMed: 26047922]

41. Anderson KE, Chessa TA, Davidson K, Henderson RB, Walker S, Tolmachova T, Grys K, Rausch O, Seabra MC, Tybulewicz VL, Stephens LR, et al. PtdIns3P and Rac direct the assembly of the NADPH oxidase on a novel, pre-phagosomal compartment during FcR-mediated phagocytosis in primary mouse neutrophils. Blood. 2010; 116:4978–4989. [PubMed: 20813901]

42. Chessa TA, Anderson KE, Hu Y, Xu Q, Rausch O, Stephens LR, Hawkins PT. Phosphorylation of threonine 154 in p40phox is an important physiological signal for activation of the neutrophil NADPH oxidase. Blood. 2010; 116:6027–6036. [PubMed: 20861461]

43. Webster J, Oxley D. Protein identification by MALDI-TOF mass spectrometry. Methods Mol Biol. 2012; 800:227–240. [PubMed: 21964792]

Europe PMC Funders Author Manuscripts

Europe PMC Funders Author Manuscripts

One-sentence summary

PI3Kγ complexes containing p101or p84 are directly activated by Gβγ in a GPCR-dependent manner in neutrophils.

Europe PMC Funders Author Manuscripts

Editor's summary

How to activate PI3Kγ in neutrophils

A critical effector of GPCRs in neutrophils is PI3Kγ, but how the two PI3Kγ complexes are activated by Gβγ has been controversial, likely due to a reliance on in vitro assays using cultured cells. Rynkiewicz *et al.* generated mice with knock-in mutations in the Gβγ-binding sites in the PI3Kγ catalytic subunit p110γ or in the regulatory subunit p101. Loss of Gβγ binding to p110γ had greater effects on signaling in response to different GPCR agonists than loss of Gβγ binding to p101. Although the migration of isolated neutrophils was affected only by loss of Gβγ binding to p110γ, neutrophil migration in mouse models of neutrophilic inflammation was strongly impaired by defective Gβγ binding to either p110γ or p101. These results refine our understanding of how PI3Kγ is activated in neutrophils and emphasize the importance of investigating signaling pathways in physiologically relevant contexts.

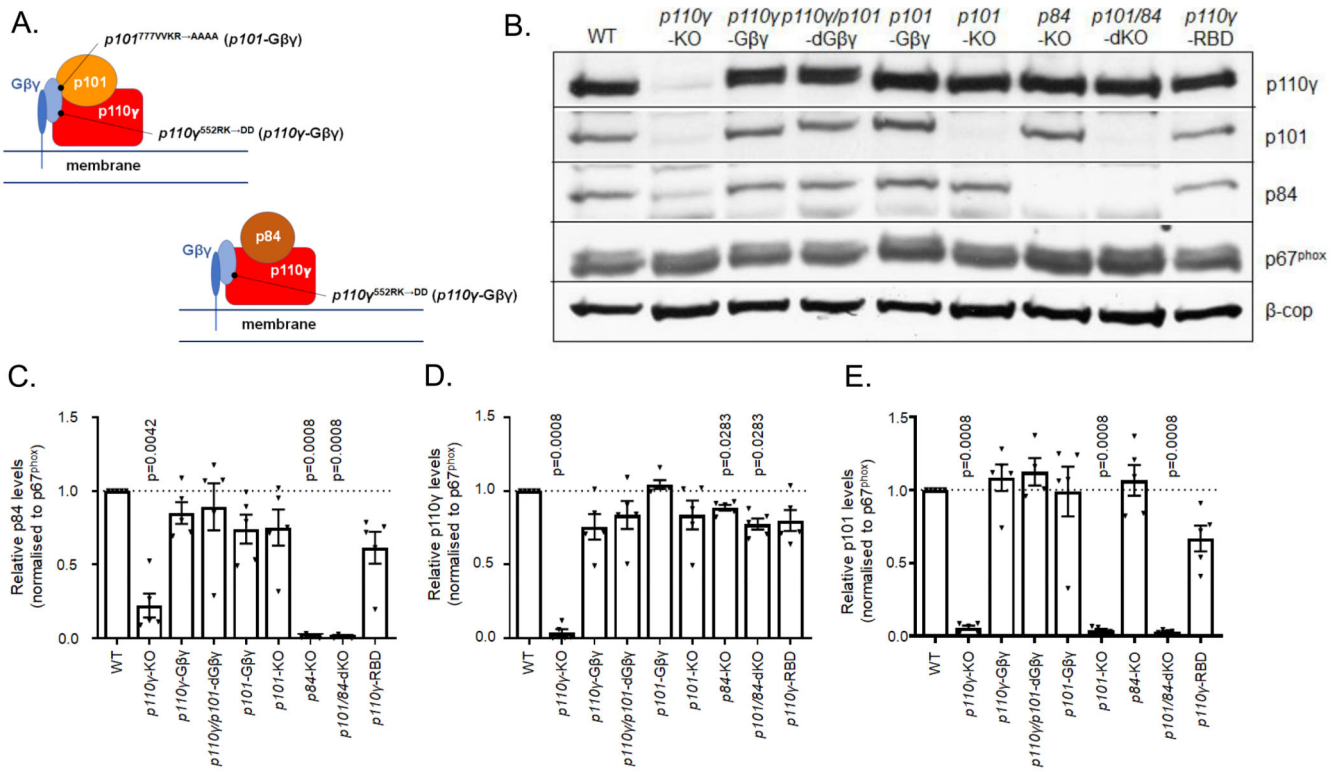

Fig. 1. Schematic diagram of mutations created in PI3Kγ subunits and their effect on expression levels in isolated bone marrow neutrophils (BMN).

(**A**) Cartoon illustrating Gβγ binding to p84-p110γ and p101-p110γ complexes and the mutations created in the Gβγ binding domains of p101 regulatory and p110γ catalytic subunits. A single Gβγ binding site is depicted in p101-p110γ but it is currently unknown whether there is a single or multiple binding sites for Gβγ in this complex. (**B** to **E**) Relative abundance of PI3Kγ subunits in BMN derived from the indicated strains of mice; (**B**) Western blot representative of five independent experiments that were combined and quantified for the abundance of p84 (**C**), p110γ (**D**) and p101 (**E**). Western blotting analysis was performed on $1x10^6$ BMNs from mice of the indicated genotypes. The abundances of p84, p110γ and p101 protein in samples from mice of each genotype were quantitated by densitometry and normalized to $p67^{phox}$ to correct for neutrophil input (β-COP is shown as an additional loading control). Data are means ± SEM of n= 5 independent experiments and are expressed as a ratio to the relative protein band density of WT samples on each blot. Normalized data was analyzed by ratio paired *t* tests with Holms-Sidak corrections applied to account for multiple comparisons, with comparisons made to WT samples.

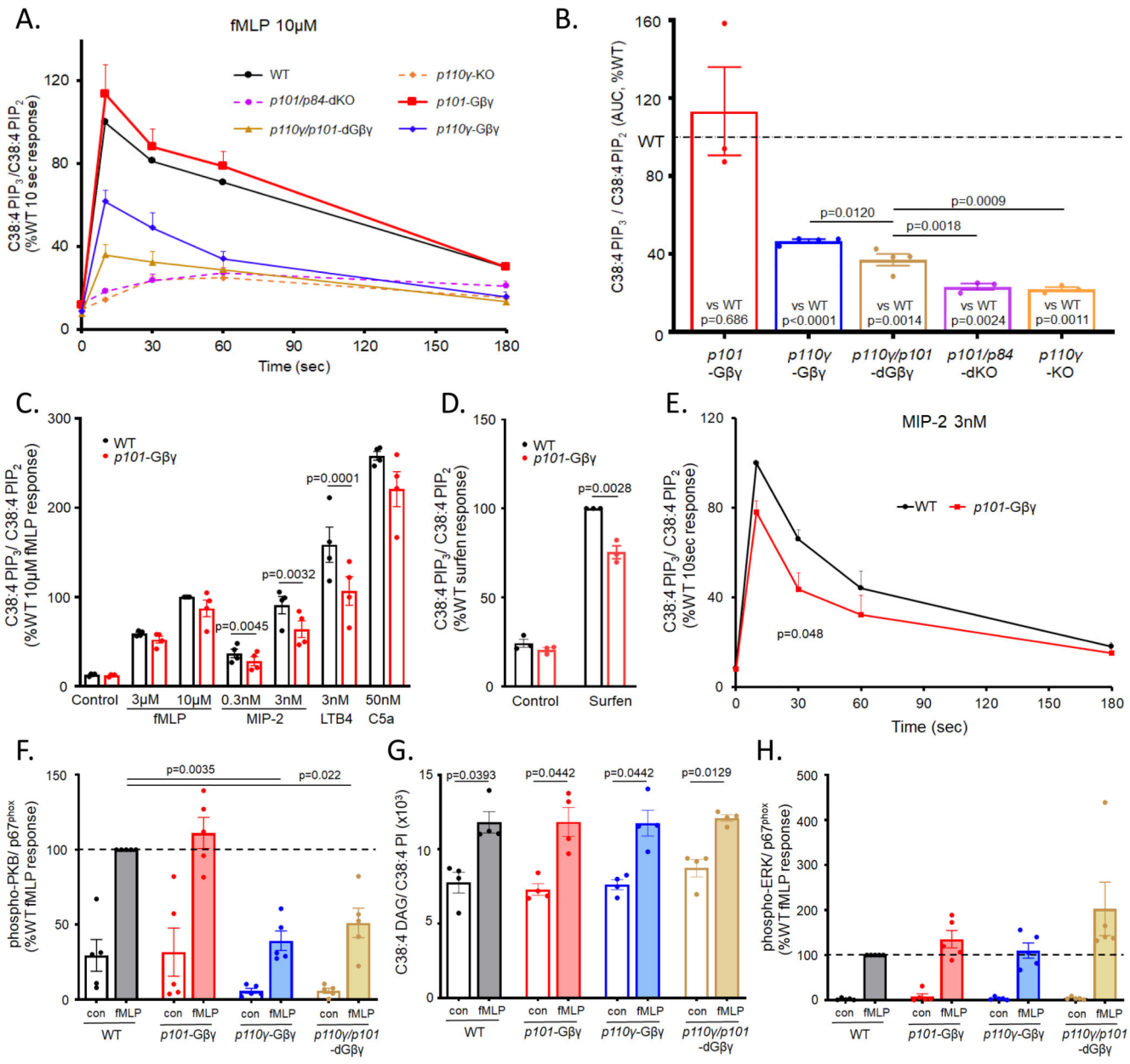

Fig. 2. GPCR-driven signaling responses in BMNs and effects of defects in Gβγ binding or knockout of PI3Kγ subunits.

(**A** and **B**) BMNs (1×10^6 cells) from *p101/p84*-dKO (dashed-purple), *p110γ*-KO (dashed-orange), *p110γ/101*-dGβγ (solid-brown), *p110γ*-Gβγ (solid-blue), *p101*-Gβγ (solid-red), and their relevant WT controls (solid-black) were stimulated at 37°C with 10μM fMLP for the indicated times. (**C**-**E**) BMNs from WT (black) and p101-Gβγ (red) mice were stimulated with indicated GPCR agonists (or vehicle controls) for 10 s (C), with 10 μM surfen (or vehicle control) for 10 min (D), or 3 nM MIP-2 for the indicated times (E). Reactions were quenched, lipids were extracted, and the amounts of C38:4-PIP_3 and C38:4-PIP_2 were quantitated by mass spectrometry. Data are means ± SEM of at least three experiments and are expressed as the ratio of the abundance of C38:4-PIP_3 to that of C38:4-

PIP_2 in the same sample (C38:4 PIP_3/C38:4 PIP_2) to account for any variations in cell input, expressed as a percentage of WT response at 10 s (A and E) or WT 10 μM *f*MLP response (C), or WT surfen response (D). (B) Areas under the curve (AUC) for *f*MLP time courses shown in (A) were calculated for each genotype response and compared to its relevant WT control in the same experiment using ratio paired *t* tests. A one-way ANOVA on log-transformed data was used for the comparisons between genotypes. Holm-Sidak correction was applied to account for multiple comparisons. Similar analysis was performed for the MIP-2 time course (E). Non-normalized data for each genotype and their relevant WT controls from (A) are shown in fig. S4. A 2-way ANOVA on log transformed data followed by Sidak's multiple comparison test was used in comparing PIP_3 responses to multiple agonists (C) whereas a *t* test was used to compare surfen PIP_3 data (D). (**F-H**) BMNs (0.5×10^6 cells) from WT (black), *p101*-Gβγ (red), *p110γ*-Gβγ (blue), and *p110γ/101*-dGβγ (brown) mice were stimulated for 1 min at 37°C with 10 μM *f*MLP. Cells were analysed for DAG (G), or lysates run on SDS-PAGE and Western blot analysis performed for phospho-PKB or ERK (F and H). Abundances of phospho-PKB and phospho-ERK protein in samples from mice of each genotype were quantitated by densitometry and normalized to total $p67^{phox}$ to correct for neutrophil input protein. A representative Western blot is shown in fig. S5. Data are means ± SEM of n≥4 independent experiments and are expressed as the ratio of abundance of C38:4-DAG to that of C38:4-PI in the same sample to account for variations in cell input (G), or as a percentage of protein band density of WT *f*MLP samples on each blot (F, H). Data was analyzed by 2-way ANOVA with Holm-Sidak correction applied to account for multiple comparisons (G) or ratio paired *t* tests with Holms-Sidak corrections applied to account for multiple comparisons, with comparisons made to WT samples (F and H).

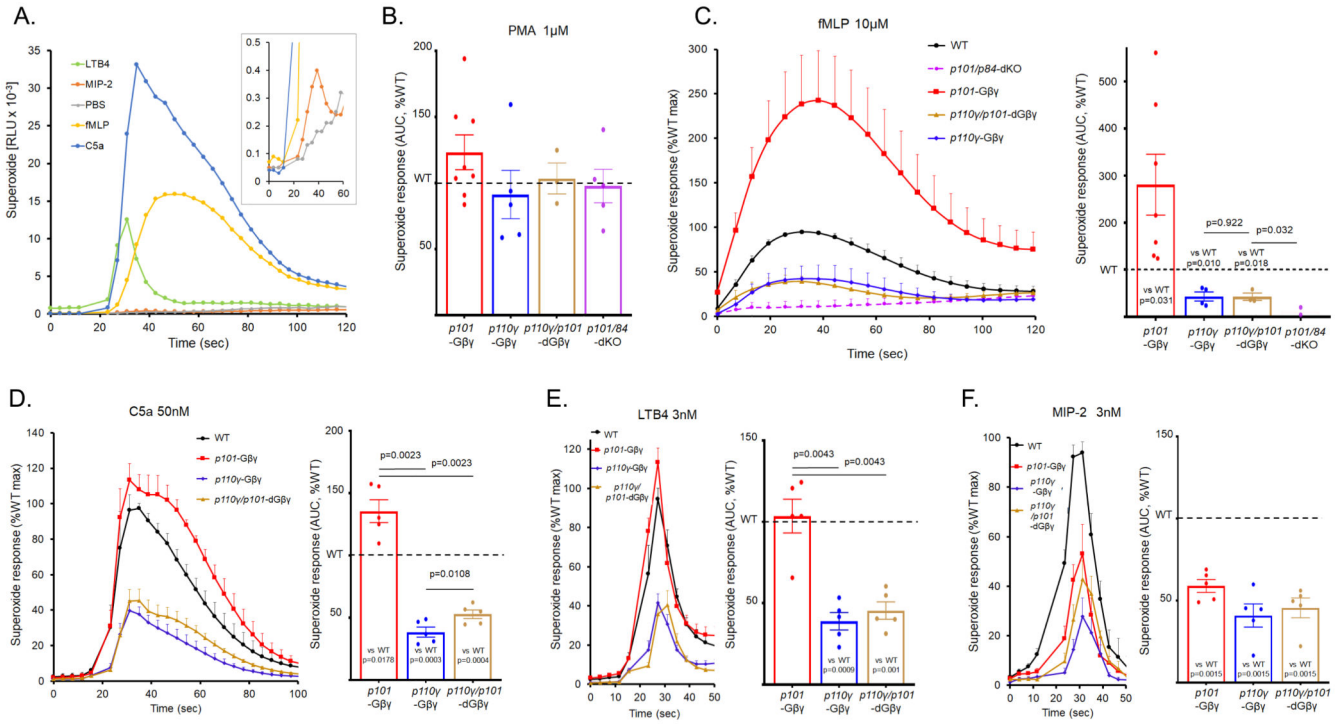

Fig. 3. Characterization of GPCR-driven superoxide responses in BMN and effects of defects in Gβγ binding or knockout of PI3Kγ subunits.

(**A-F**). BMNs (0.5×10^6) from *p110γ/101*-dGβγ, *p101*-Gβγ, *p110γ*-Gβγ, or *p101/p84*-dKO mice, and their relevant WT controls, were preincubated with horseradish peroxidase (HRP) and luminol before being added to a 96-well plate. Agonists were either injected (A and D to F) or manually added to wells (B and C). ROS generation was then measured in duplicate for each genotype by chemiluminescence and recorded with a Berthold MicroLumat Plus luminometer. Data are means ± SEM for accumulated light emission (RLU) per second (A and C to F, left hand panels**)** for at least three experiments (except for *p101/p84*-dKO where n=3 experiments for PMA stimulation and n=2 experiments for fMLP stimulation (B and C)); data were normalized to the WT maximal response for each experiment (C to F, left hand panels) or accumulated ROS over the recording times, expressed as a percentage of accumulated ROS in WT cells (B to F right hand panels). Non-normalized superoxide responses from each genotype were compared to their relevant WT control in the same experiment using ratio paired *t* tests. A one-way ANOVA on log-transformed data was used for the comparisons between genotypes. Holm-Sidak correction was applied to account for multiple comparisons. Non-normalized data for each genotype and relevant WT control (C) are found in fig. S5.

Europe PMC Funders Author Manuscripts

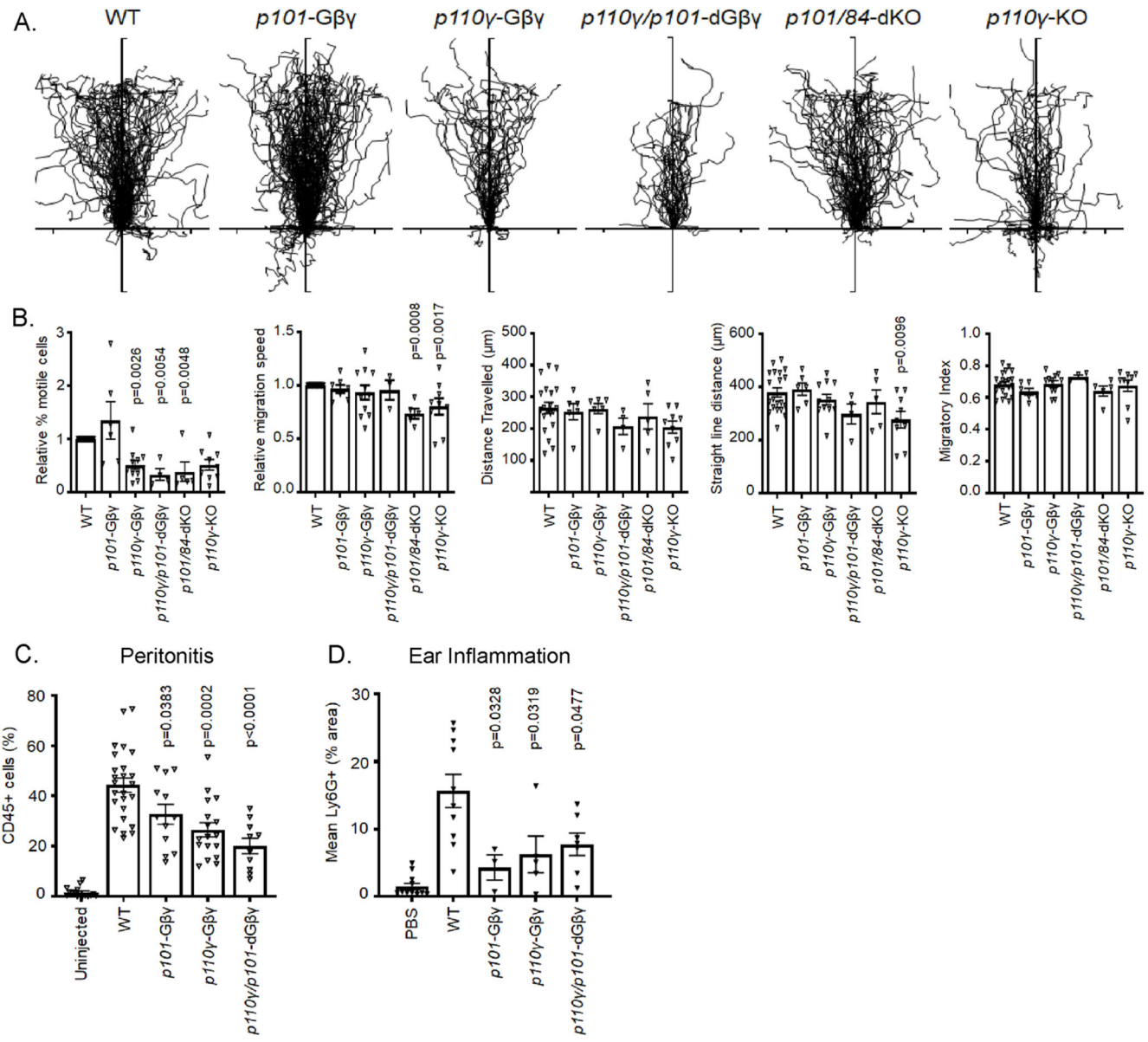

Fig. 4. Effect of Gβγ binding to PI3Kγ subunits on BMN migration in vitro and in in vivo models of inflammation.

(**A**). Centre-zeroed tracks of individual WT, *p101*-Gβγ, *p110γ*-Gβγ, *p110γ/10*1-dGβγ, *p101/p84*-dKO or *p110γ*-KO BMNs in an EZ-Taxiscan Chamber migrating towards reservoirs located at the top of the diagrams containing 3 μM *f*MLP. Isolated cells were added to chambers containing fibrinogen-coated glass coverslips. Shown are combined data from at least 4 experiments with at least 9 tracks per experiment. (**B**). Analysis of EZ-Taxiscan migratory tracks showing relative percentage of migratory cells and migration speed normalized to WT values (WT migration 31.9 ± 2.8% of cells, WT velocity 11.4 ± 0.44 μm/min), distance travelled, straight line distance and migratory index. Thirty five to 250 cells were analyzed for each genotype in each experiment. Data are mean ± SEM of average track data from each experiment. Data were analyzed by one-way ANOVA followed

by Dunnett's multiple comparison test, comparing each genotype against WT data. **(C)** Mice of the indicated genotypes were injected with 3% thioglycolate (I.P.) or left uninjected. 3.5hours later the peritoneum was flushed and cells collected for FACS analysis gating for CD45+ cells. Quantitation of other cell types in the peritoneum flush in the absence or presence of thioglycolate-induced peritonitis are shown in fig. S6. (**D**) For ear-pouch inflammation models, anesthetised mice of the indicated genotypes were injected with either 1.5 μM MIP-2 or vehicle intradermally in the pinna (until a blister about 4 to 5 mm in size formed) and mice were sacrificed 4 hours later. The pinna was stained with Ly6G, and the extent of Ly6G staining was evaluated by microscopy with at least 10 images taken from each pinna. In (C) and (D), BMN accumulation from *p101*-Gβγ, *p110γ*-Gβγ, or *p110γ/101*-dGβγ mice, and their relevant WT controls was quantitated using FACS analysis and data shown are mean ± SE from at least three mice per genotype group. Data were analyzed by one-way ANOVA followed by Dunnett's multiple comparisons test, comparing each genotype to WT data.

Europe PMC Funders Author Manuscripts